Journal of ELECTRONIC MATERIALS, Vol. 48, No. 9, 2019
https://doi.org/10.1007/s11664-019-07373-6

Piezoelectric and Dielectric Properties of (0.970(0.95($K_{0.485}Na_{0.515}$) NbO_3-0.05$LiSbO_3$)-0.015CuO-0.015Al_2O_3)/PVDF Composites at Different Immersing Conditions

KUN YU,[1,3] SHAN HU ,[1,2,4] WENDI YU,[1,5] and JUNQIN TAN[1,6]

1.—Faculty of Materials Science and Chemistry, China University of Geosciences, No. 388, Lumo Road, Hongshan District, Wuhan City 430074, Hubei Province, People's Republic of China. 2.—Engineering Research Center of Nano, Geomaterials of Ministry of Education, China University of Geosciences, Wuhan 430074, People's Republic of China. 3.—e-mail: ujo7400673@163.com. 4.—e-mail: hushan@cug.edu.cn. 5.—e-mail: 771267404@qq.com. 6.—e-mail: 1484646698@qq.com

(KNNLS-CA)/PVDF composites were fabricated by a hot-pressing process using 0.970(0.95($K_{0.485}Na_{0.515}$) NbO_3-0.05$LiSbO_3$)-0.015CuO-0.015Al_2O_3 (KNNLS-CA) ceramic powder and polyvinylidene fluoride (PVDF). The crystalline structures, morphology, densities, conductivity, dielectric and piezoelectric properties of (KNNLS-CA)/PVDF 0–3 composites were investigated. It is found that the phase structure is perovskite with orthorhombic symmetry for KNNLS-CA ceramic. When the ceramic content is 60 wt.%, the lattice strain reaches the maximum value. In addition, the ceramic particles can increase the relative fraction of the β-phase and restrain α-phase in PVDF matrix. By immersing the samples under different conditions (de-ionized water and NaOH/KOH solutions), it is found that K^+ ions are easier to form electrolytes and enhance the dielectric properties. Water solution can delay the neutralization between alkali metal ions especially Na^+ ions and space charges, and improve the piezoelectric properties. In this study, a dielectric constant as ultrahigh as 185723 is obtained at 0.2 M KOH (aq) (100 Hz), which is about 928 times higher than that of the untreated composites. The dielectric properties are well explained in terms of an interfacial percolation model. The piezoelectric coefficient as high as 75 pC/N is obtained at 0.05 M NaOH (aq) and increases more than 97% of that of untreated samples. All samples have good piezoelectric stability.

Key words: KNNLS-CA, PVDF, 0–3 composite, dielectric properties, piezoelectric properties

INTRODUCTION

Researchers once thought that the most ideal piezoelectric material was lead zirconium titanate ceramic. However the use of this material has been restricted in many areas owing to its toxicity. On the other hand, lead-free piezoelectric ceramics have been widely studied. Among various lead-free materials, potassium sodium niobate (KNN) has lots of advantages such as high piezoelectric constant, environment-friendly material, high Curie temperature ($T_c > 400°C$), etc. Hence, KNN ceramic is widely used in electromechanical transducers, sensors, actuators and other electronic devices.[1] Recently, many researchers synthesized KNN

(Received March 5, 2019; accepted June 11, 2019; published online June 18, 2019)

series ceramics by using the conventional solid state reaction and obtained high d_{33} values.[2–4] Its piezoelectric property is comparable to that of lead zirconium titanate ceramic. Nonetheless, as a common problem of ceramic material, repeated processing which leads to serious performance degradation can limit its application. Therefore, researchers have proposed to add polymer material into ceramic in order to improve the properties mentioned above. Among all kinds of polymer materials, PVDF possesses many excellent properties, such as outstanding low thermal conductivity, light weight and low cost.[5] Pure PVDF is a semicrystalline polymer, and it has five polymorphic forms, namely α, β, γ, δ, and ε. The two important ones are the nonpolar α-phase and the polar β-phase.[6] The content of β-phase in PVDF is considered to be an important factor affecting the piezoelectric property. In addition, PVDF polymer also has some disadvantages, such as high loss tangent, low values of piezoelectric coefficient (d_{33}~20 pC/N) and dielectric constant (ε_r~6).

Considering the 0–3 type connected composite is easier to prepare than the others types (0–0, 0–3, 1–2, etc.) composite, and the filler shows a good dispersion in the matrix,[7] the 0–3 type connected composite method in this study was used. Moreover, the post-treatment process also has a great impact on the properties of the composites, especially the dielectric properties. At present, hot-pressing, cold-pressing and electrospinning methods are commonly used in the post-treatment process.[8,9] The cold-pressing method that was reported in the literature generally produces small holes and high loss tangent in the composites.[10] In addition, the electrospinning method is too complex for large-scale production. The hot-pressing method is widely used by more and more researchers because of its advantages such as easy operation, high performance of composite and so on.[11–13]

In most studies, the samples are placed in air for 24 h after polarization. According to Zhang's research, the samples are placed in de-ionized water after polarization and then tested after drying, it is found that the samples can greatly improve the d_{33} and ε_r due to the effect of interfacial percolation.[10] According to the research of Jarkko and Goyal, when graphite is added to ceramic or composite, it can produce lots of conducting particles to form conducting channels and increases the dielectric constant and loss tangent.[14,15] However, the effect of alkali solution on the electrical properties of sample is rarely reported.

From the above, in this work, (KNNLS-CA)/PVDF lead-free 0–3 composites were fabricated by hot-pressing. The crystal structures, microstructures were studied respectively. After polarization, these samples were treated in air, de-ionized water, NaOH/KOH solutions. The electrical properties were investigated systematically.

EXPERIMENTAL

The $0.970(0.95(K_{0.485}Na_{0.515})NbO_3\text{-}0.05LiSbO_3)\text{-}0.015CuO\text{-}0.015Al_2O_3$ powder was prepared by a conventional solid-state reaction route. The raw materials were K_2CO_3 (Aldrich 99.99%), Na_2CO_3 (Aldrich 99.8%), Li_2O_3 (Aldrich 99%), Nb_2O_5 (Aldrich 99.9%), Sb_2O_3 (Aldrich 99.5%), CuO (Aldrich 99%) and Al_2O_3 (Aldrich 99%). These materials were dried at 60°C for 24 h to remove moisture and weighted according to their stoichiometric formulae. Then the materials were ball-milled for 24 h in absolute ethyl alcohol with zirconia balls to obtain a homogenous mixture. The mixture was dried and calcined at 850°C for 3 h in a covered alumina crucible. After calcination, the powder was crushed and ball-milled again for 24 h. After drying, the powder was mixed with 5 wt.% polyvinyl alcohol (PVA) as binder and pressed into disks of 14 mm in diameter and about 1 mm in thickness at 10 MPa. The disks were buried in alumina powder and heated at 650°C for 5 h in order to remove the PVA polymer. Subsequently, the disks were sintered in a temperature at 1050°C for 3 h in ambient atmosphere and crushed into powder by a high speed mill.

PVDF polymer was provided by Shanghai 3F Co.,China. The PVDF polymer and KNNLS-CA powder were mixed in absolute ethyl alcohol. At this step, the weight fractions of ceramic were varied from 40 wt.% to 80 wt.%. The mixture was continuously stirred by using a magnetic stirrer at 500 rpm at 70°C for 30 min and evenly ultrasonically dispersed at 60°C for 30 min. The mixture was dried at 100°C for 24 h. The dried powder then pressed into disks of 14 mm in diameter and about 1 mm in thickness at 10 MPa. After that, the disks were heated by hot-pressing at 200–220°C for 10 min and polished. In order to measure the electrical properties, the samples were coated with silver paste as electrodes and kept inside an oven at 80°C for 2 h to form electrodes. The samples were carried out at 100°C in a silicone oil bath by applying a DC field of 3–6 kV/mm for 30 min. Later, the samples were placed in different conditions for 24 h, such as air atmosphere, the deionized water and NaOH and KOH solutions (0.05 M, 0.1 M and 0.2 M). Then the dielectric constant ε_r, conductivity σ and piezoelectric coefficient d_{33} of the samples were measured directly after taking the samples out from different conditions and drying for 3 h at 60°C.

The crystalline structures and phases of the KNNLS-CA powder, pure PVDF and (KNNLS-CA)/PVDF composites samples were subsequently determined by using a Bruker AXS D8-Focus (Germany) with *Cu* $K\alpha$ radiation. The FTIR spectra of the samples were performed by using a Thermo Nicolet Corporation NEXUS 670 (USA). The fractured surface microstructural images were carried out at room temperature by using a Hitachi SU-8010 (Japan). The piezoelectric coefficient d_{33} was

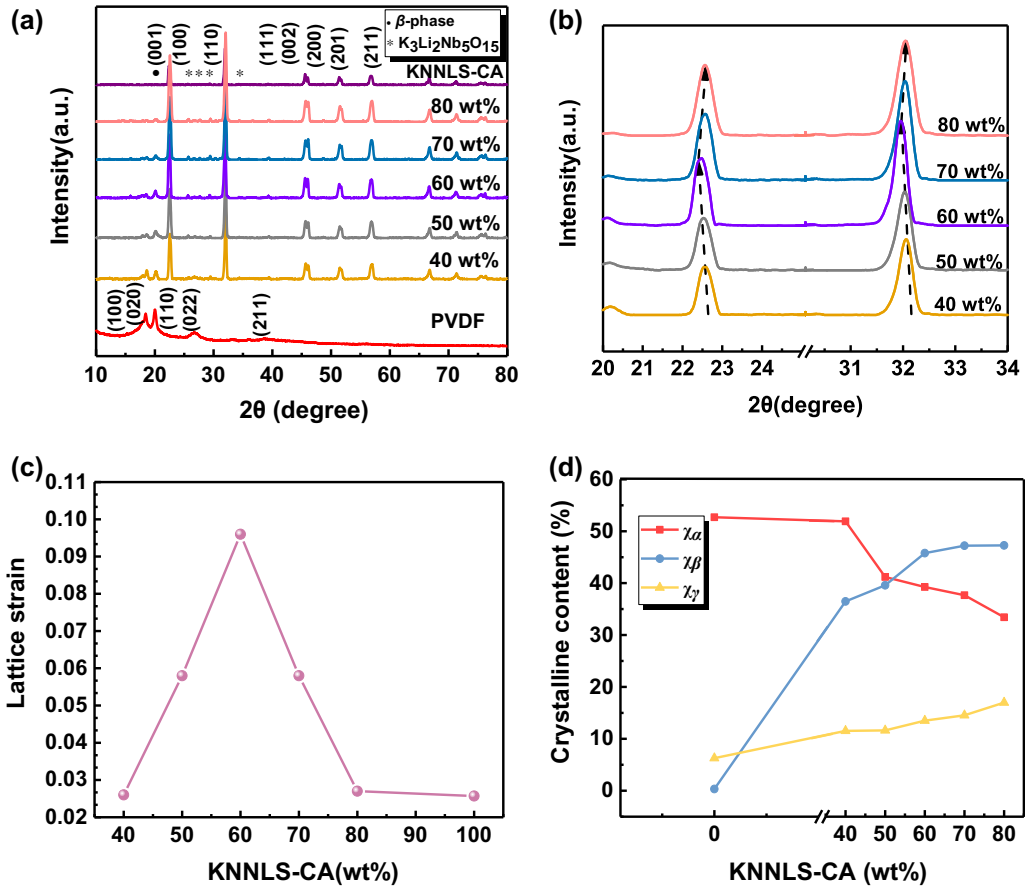

Fig. 1. (a) XRD patterns of pure PVDF polymer, KNNLS-CA powder and (KNNLS-CA)/PVDF composites. (b) The enlarged XRD patterns of the composites in the range from 20° to 25° and 31° to 34°. (c) Plot of lattice strain versus content of KNNLS-CA. (d) The variation in the amount of α-phase, β-phase and γ-phase in PVDF.

measured by using a Piezotest PM-200 (UK) at 110 Hz. The dielectric properties and conductivity σ were determined by using a Keysight Technologies E4990A (USA). The bulk density was measured by a DahoMeter DE-200 M (China).

RESULTS AND DISCUSSION

X-ray Structure Analysis

Figure 1a shows the XRD patterns of pure PVDF, KNNLS-CA ceramic and the composites of different weight fractions of ceramic. The x-ray pattern of pure PVDF represents a typical semi-crystalline structure composed of α-phase (the peaks at 2θ corresponding to (100), (020)), β-phase (the peak at 2θ corresponding to (110) and γ-phase (the peaks at 2θ corresponding to (022) and (211)).[16–18] The peaks corresponding to α-phase, β-phase and γ-phase are weakened with the increase of KNNLS-CA content and obviously the XRD patterns of composites mainly show the peaks of KNNLS-CA ceramic. The peak intensity between 45.2° (002) and 46° (200) is compared as shown in Fig. 1a, it is found that the phase structure of ceramic is perovskite with orthorhombic symmetry for all composites and KNNLS-CA ceramic.[19] In addition, the peaks for $K_3Li_2Nb_5O_{15}$ (PDF#52-0157) second phase with tetragonal tungsten-bronze structure are also detected in all composites and KNNLS-CA ceramic from Fig. 1a. Because of the different ionic radius and valence, the addition of CuO can result in lattice distortion and the instability of the perovskite structure. Li^+ ions diffuse into lattices and occupy the triangular spaces in tungsten-bronze structure owing to the lower radius, generate $K_3Li_2Nb_5O_{15}$ s phase.[20] According to the researches of Chen and Guo, $K_3Li_2Nb_5O_{15}$ was detected in KNN ceramics with Li-rich compositions when the solid solubility of Li was about 3 mol.%.[21,22] It clearly observed that the Li-doping content exceeded 3 mol.% in the 0.970(0.95(K0.$_{485}$$Na_{0.515}$) NbO_3-0.05$LiSbO_3$)-0.015CuO-0.015Al_2O_3 system. Furthermore, the formation of $K_3Li_2Nb_5O_{15}$ indicates that some K^+ and Li^+ ions cannot occupy the A-sites in KNNLS, and resulting in many vacancies.[22] In order to keep the charge balance, many oxygen vacancies are generated. At the same time, Cu^{2+} ions can enter into a B site in this ABO_3 perovskite structure and substitute Nb^{5+} ions (B-sites). This also can produce oxygen vacancies and improve the electrical conductivity and mechanical quality factor Q_m of ceramics.

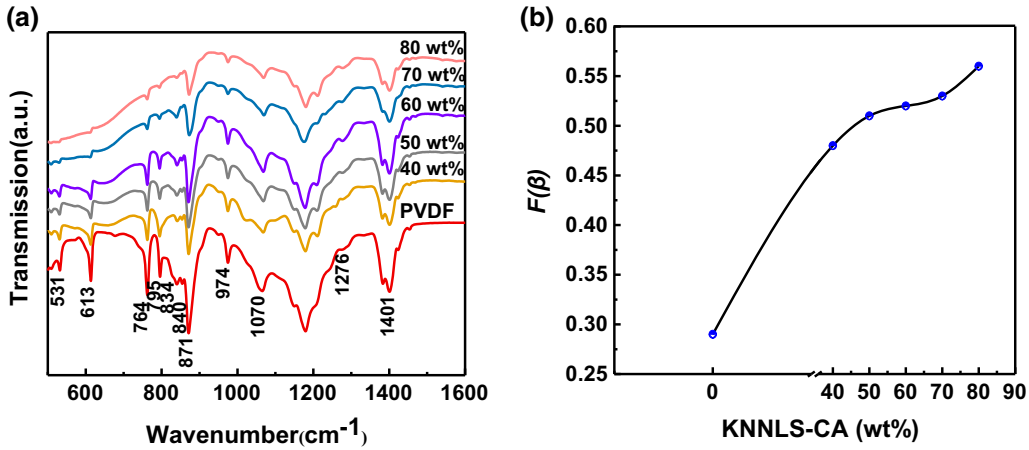

Fig. 2. (a) FTIR spectra of pure PVDF polymer and (KNNLS-CA)/PVDF composites. (b) The ratios of β-phase in the pure PVDF polymer and (KNNLS-CA)/PVDF composites.

The average crystallite size can be calculated by using Scherrer's formula as the following Eq. 1:

$$D = \frac{k\lambda}{\beta_{\mathrm{FWHM}} \cos\theta}, \tag{1}$$

where β_{FWHM} is the full width at half maximum (FWHM) diffraction peak, k represents a shape factor, and it is taken to be 0.89, λ is 0.1542 nm which is the wavelength of Cu K_α source, θ is the peak position. When the KNNLS-CA content is 40%, 50%, 60%, 70% and 80%, the crystallite size is 20.0 nm, 16.0 nm, 25.9 nm, 15.4 nm and 14.0 nm, respectively.

The enlarged XRD patterns of the composites in the range from 20° to 25° and 31° to 34° are shown in Fig. 1b. As shown in Fig. 1b, the Bragg's diffraction angle reached the minimum value when the ceramic content is 60 wt.%. Therefore, it demonstrates that the lattice parameters reached the maximum value at 60 wt.% ceramic. The lattice strain is introduced to explain the change of lattice parameters. The lattice strain can be calculated by the Williamson-Hall plot method which can be expressed as Eq. 2:

$$\beta \cos\theta = \frac{k\lambda}{D} + 4\varepsilon \sin\theta, \tag{2}$$

where ε is lattice strain and $4\varepsilon\sin\theta$ represents strain effect on the crystallites. Generally, in the process of drawing the Williamson-Hall plot, $\frac{4\sin\theta}{\lambda}$ is used as the horizontal coordinate and $\frac{\beta\cos\theta}{\lambda}$ is used as the vertical coordinate. The least square method is used for line fitting. The slope of the line is strain, and the intercept of the line on the ordinate is the reciprocal of the crystallite size. These values of lattice strain are shown in Fig. 1c. The lattice strain increases with the content of KNNLS-CA increasing and reaches its maximum 0.096 when the ceramic content is 60 wt.%. But the lattice strain decreases when the ceramic content exceeds 60 wt.% and reaches the minimum value 0.0257 when the ceramic content is 100 wt.%. In consequence, it concludes that the maximum strain tolerance in the composites was obtained at 60 wt.% ceramic content. In addition, according to the Williamson-Hall plot method (Eq. 2), the average crystallite size is 17.0 nm, 15.9 nm, 21.8 nm, 13.9 nm and 12.8 nm, respectively. It should be noted that both methods show the same grain-size trend. The reason for decrease in crystallite size with KNNLS-CA contents (40 wt.% to 50 wt.% and 60 wt.% to 80 wt.%) may be due to the hot pressing. The PVDF polymer can obtain the curl when the hot pressing is used, and the KNNLS-CA grains are wrapped by the PVDF polymer, which indicates the connection characteristic of 'wrap and curl', the connection between the grains of composite prepared by hot pressing is much closer and the crystallite size is also smaller.[8] In addition, the other reason for decrease in crystallite size with ceramic content (especially 40 wt.% to 50 wt.%) is the formation of new defects particularly dislocations. It might result in formation of high dislocation density regions into the grains and pile up the grain boundaries or irregular clusters into the grains. Therefore, it results in reduction of crystallite size.[23] However, the reason for increase in crystallite size with KNNLS-CA content (50 wt.% to 60 wt.%) is not clear, many studies have shown that strain is inversely proportional to crystallite size,[24–26] few reports have been found in the literature on these discoveries about the strain is proportional to crystallite size,[27] we presume that this phenomenon may be due to the lattice strain. On the other hand, the crystallite size obtained by the Scherrer formula is greater than those obtained by the Williamson-Hall method. This result is in agreement with the previous research reported by P Kour.[28] The Scherrer's formula is generally applicable to the calculation of particles with a crystallite size of less than

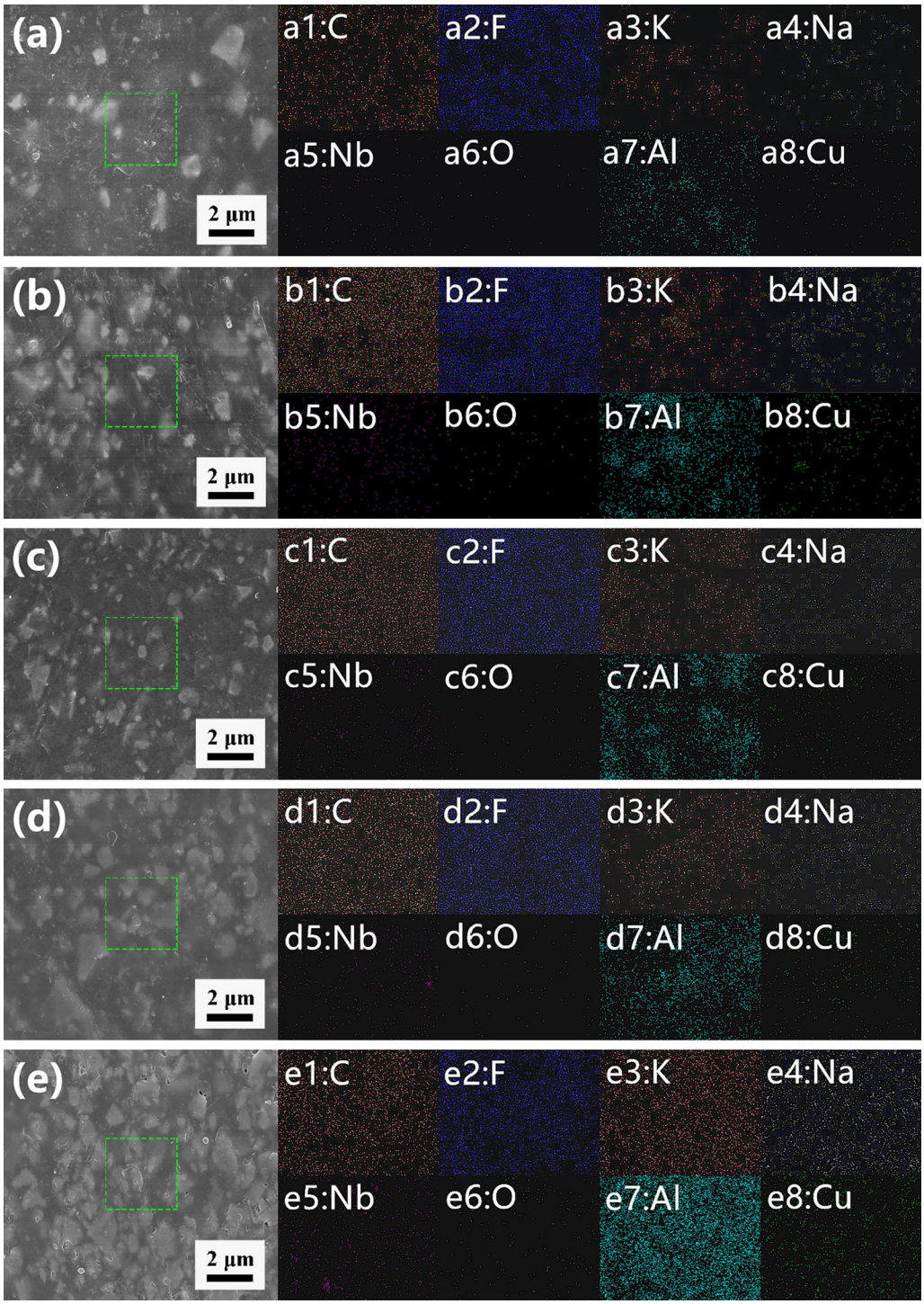

Fig. 3. SEM images of the fractured surfaces of the composites with KNNLS-CA content of (a) 40 wt.%, (b) 50 wt.%, (c) 60 wt.%, (d) 70 wt.%, and (e) 80 wt.%. The elemental mapping results of all samples: (a1)–(a8), (b1)–(b8), (c1)–(c8), (d1)–(d8) and (e1)–(e8) correspond to the red rectangle area in (a), (b), (c), (d) and (e), respectively.

100 nm. When the crystallite size is less than 100 nm, the stress-induced broadening is negligible compared to the broadening caused by the crystallite size. At such conditions, the Scherrer's formula is reasonable. However, when the crystallite size is large to a certain value (above 100 nm), the stress-induced broadening is significant. In this condition, the widening caused by strain must be considered, and the Scherrer formula is no longer applicable. Although the crystallite size in this system is less than 100 nm and the Scherrer's formula can be used to calculate the crystallite size, the strain correction factor has been taken into account in the case of the Williamson-Hall method whereas it has not been

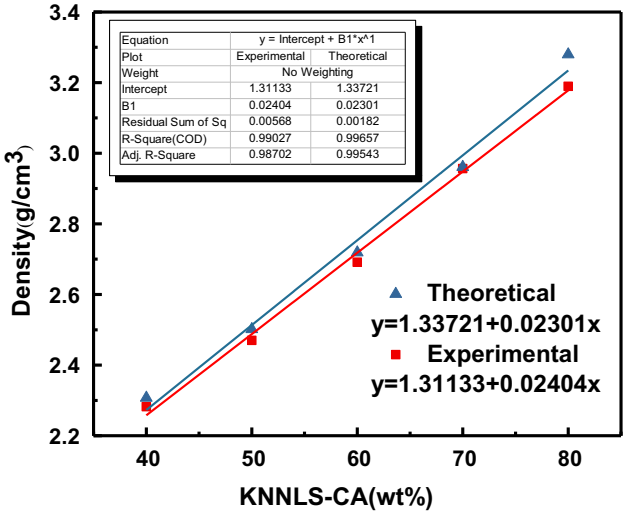

Fig. 4. Variation of the density with KNNLS-CA content in the composites.

taken into account in Scherrer's method.[29] Therefore, the crystallite size obtained by the Williamson-Hall methods are more accurate in this system.

Because of the existence of dipoles formed by carbon bond and fluorine in β-phase structure, PVDF polymer exhibits piezoelectric characteristics. In order to quantify the main phases crystalline contents in composite, the contents of each phase, $\chi_{\alpha,\beta,\gamma}$, can be described by Eq. 3:

$$\chi_{\alpha,\beta,\gamma} = \frac{A(\alpha,\beta,\gamma)}{A(\alpha+\beta+\gamma)}, \tag{3}$$

where $A(\alpha,\beta,\gamma)$ is the area of characteristic peaks of α-phase, β-phase and γ-phase. The variation in the amount of these phases in pure PVDF and composites has been shown in Fig. 1d. It can be clearly seen that when the ceramic content increases, the contents of β-phase and γ-phase gradually increase but the content of α-phase decreases. This may be due to the transformation of α-phase into β-phase and γ-phase. Hence, the piezoelectric properties of PVDF also can increase when ceramic particles are added in PVDF.

FOURIER TRANSFORM INFRARED (FTIR) ANALYSIS

Figure 2a shows the FTIR spectra of pure PVDF polymer and (KNNLS-CA)/PVDF composites in the wave number range of 500–1600 cm^{-1}. The bands at 531 (CF_2 bending), 613 (CF_2 bending and skeletal bending of C(F)-C(H)-C(F)), 764 (CF_2 bending and skeletal bending of C(F)-C(H)-C(F)), 795 (CH_2 rocking) and 974 cm^{-1} (CH_2 bending mode) correspond to the α-phase. The modes at 840 (CH_2, CF_2 rocking and asymmetric stretching), 871 (CC skeletal), 1070 (CC skeletal), 1276 (CF_2 skeletal) and 1401 cm^{-1} (CF_2 wagging) correspond to the β-phase. The band at 834 cm^{-1} is considered to be the signature of γ-phase (C–C stretching), which correspond to

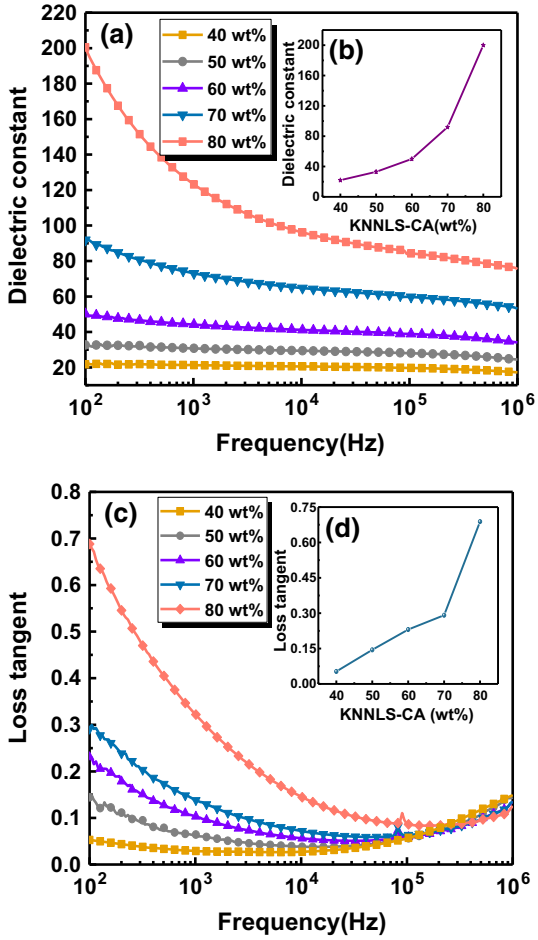

Fig. 5. Frequency dependence of (a) dielectric constant and (c) loss tangent of (KNNLS-CA)/PVDF composites with different weight fractions. (b) Dielectric constant and (d) loss tangent of (KNNLS-CA)/PVDF composites with different weight fractions at 100 Hz.

TTTGTTG'.[30,31] On the other hand, it is found that the intensities of the peaks at 531, 613, 764, 795 cm^{-1} which belong to the α-phase decreases in all composites. Therefore, KNNLS-CA ceramic particles can modify the contents of phases in PVDF. This result is found to be in close agreement with the XRD data (Fig. 1d). To evaluate the ratio of the β-phase in each sample, the following Eq. 4 has been used to calculate it:

$$F(\beta) = \frac{X_\beta}{X_\alpha + X_\beta} = \frac{K_\beta}{(K_\alpha + K_\beta)A_\alpha + A_\beta} = \frac{A_\beta}{1.26A_\alpha + A_\beta}, \tag{4}$$

where X_α is crystalline mass fraction of the α-phase, X_β is crystalline mass fraction of the β-phase. K_α and K_β represent the absorption coefficient 6.1×10^4 and 7.7×10^4 respectively. A_α and A_β are the absorbency in FTIR spectrum corresponding to 764 and 840 cm^{-1}.[32,33] Figure 2b shows the variation of $F(\beta)$ of (KNNLS-CA)/PVDF composites. The ratio of the β-phase is found to increase with increasing ceramic content. When the ceramic content is

80 wt.%, the $F(\beta)$ value of the composite is 56%. Therefore, the KNNLS-CA ceramic particles can increase the ratio of the β-phase in PVDF and may enhance the piezoelectric property.

Micro-structural Characterization

SEM technique can distinguish a presence of fillers, the phase separation, microvoids and functional groups present in the composite system. Figure 3 shows the SEM images of fractured surfaces of the composites with various KNNLS-CA contents. The density of grains increases as a function of KNNLS-CA content and the particle size of KNNLS-CA ceramic estimated from Fig. 3a–e is approximately 0.2–1.5 μm. We found that PVDF polymer minimizes the cracking of the KNNLS-CA particles due to PVDF having a relatively high elasticity compared to KNNLS-CA. Thus, the grain size and the composition of (KNNLS-CA)/PVDF may be influenced by the content of PVDF polymer.[34] It also can be obviously observed that the KNNLS-CA ceramic grains can be well dispersed in PVDF matrix in the form of a typical 0–3 composite structure, but there are some agglomerations of the KNNLS-CA particles from Fig. 3e. The SEM micrograph of 80 wt.% KNNLS-CA ceramic demonstrates some irregular pores are randomly distributed on the surface of (KNNLS-CA)/PVDF composite. In order to further confirm the PVDF polymer and KNNLS-CA ceramic distribution in composite, the energy-dispersive x-ray spectroscopy (EDS) was used to investigate (shown on the right side in Fig. 3). It can be observed that there is successful incorporation of Al_2O_3 and CuO particles into the composite. However, the Li element cannot be observed by EDS technique due to its light weight. On the whole, these images indicate the homogeneous distribution of most elements.

Density

The experimental density of (KNNLS-CA)/PVDF composites was obtained by the Archimedes principle. According to the mixture rule of composite materials, the theoretical density of (KNNLS-CA)/PVDF composites can be estimated by Eq. 5:

$$\rho = V_c\rho_c + (1 - V_c)\rho_m, \tag{5}$$

where ρ is the theoretical density, V_c is the volume fraction of KNNLS-CA ceramic, ρ_c is the experimental density of KNNLS-CA ceramic (4.197 g/cm^3), and ρ_m is the density of PVDF matrix (1.750 g/cm^3). The volume fraction V_c of KNNLS-CA ceramic is calculated by the following Eq. 6:

$$V_c = \frac{W_c}{W_c + W_p(\rho_c + \rho_m)}, \tag{6}$$

where W_c is the weight fraction of KNNLS-CA ceramic particles while W_p is the weight fraction and the experimental density of PVDF polymer. By calculation, the weight fraction is 40, 50, 60, 70 and 80% that corresponds to the volume fraction of 21.8, 29.4, 38.5, 49.3 and 62.5%, respectively. The experimental and theoretical densities are shown in Fig. 4. The experimental density can reach 97%-99% of the theoretical density due to hot-pressing technique. This phenomenon probably owing to the PVDF polymer can fill the gaps and pores in composite by hot-pressing conditions, and the homogenous distribution of KNNLS-CA ceramic in composite at lower weight fraction. However, when the KNNLS-CA content reaches 80%, the experimental density decreases to 97% of the theoretical density. This is attributed to some agglomeration of KNNLS-CA ceramic at higher weight fraction. At the same time, PVDF content is too little to be wrapped around ceramic particles, and leads to more holes and defects between the ceramic particles. This also corresponds to the above analysis of SEM images (Fig. 3e). By the linear fit to the data, it can be found that the R-Square of both fitting equations reaches 99%. In other words, the experimental density can be well predicted by the fitting equation.

Dielectric and Piezoelectric Properties

Dielectric Properties

Figure 5 shows the dielectric constant (ε_r) (Fig. 5-a) and the loss tangent ($tan\delta$) (Fig. 5c) of (KNNLS-CA)/PVDF composites as a function of frequency which range from 10^2 Hz to 10^6 Hz at room temperature (Air). As many studies report that,[35,36] the dielectric constant and loss tangent decrease with increment of frequency, and increase with ceramic content in the composites. This phenomenon reflects the dielectric response (a strong frequency dispersion) is the main characteristic of relaxor ferroelectrics.[37,38] The dielectric constant usually keeps a high value at low frequency which is due to the dipole steering polarization, electron polarization, ionic displacement polarization, space charge polarization and relaxation polarization. The space charge polarization is the dominating factor in these polarizations.[39] The loss tangent usually keeps a high value at low frequency due to an accumulation of free charge. As the frequency increases, the dipole steering polarization, ionic displacement polarization and relaxation polarization are gradually discontinued, space charge carriers, which play a major role in space charge polarization, cannot respond to the applied electric field fast enough, so the effect of space charge polarization is also gradually weakened.[40] Hence, the dielectric constant and loss tangent decrease with increment of frequency, moreover, only weak dipole steering polarization and electron polarization can exist at high frequency.[41] Furthermore, in

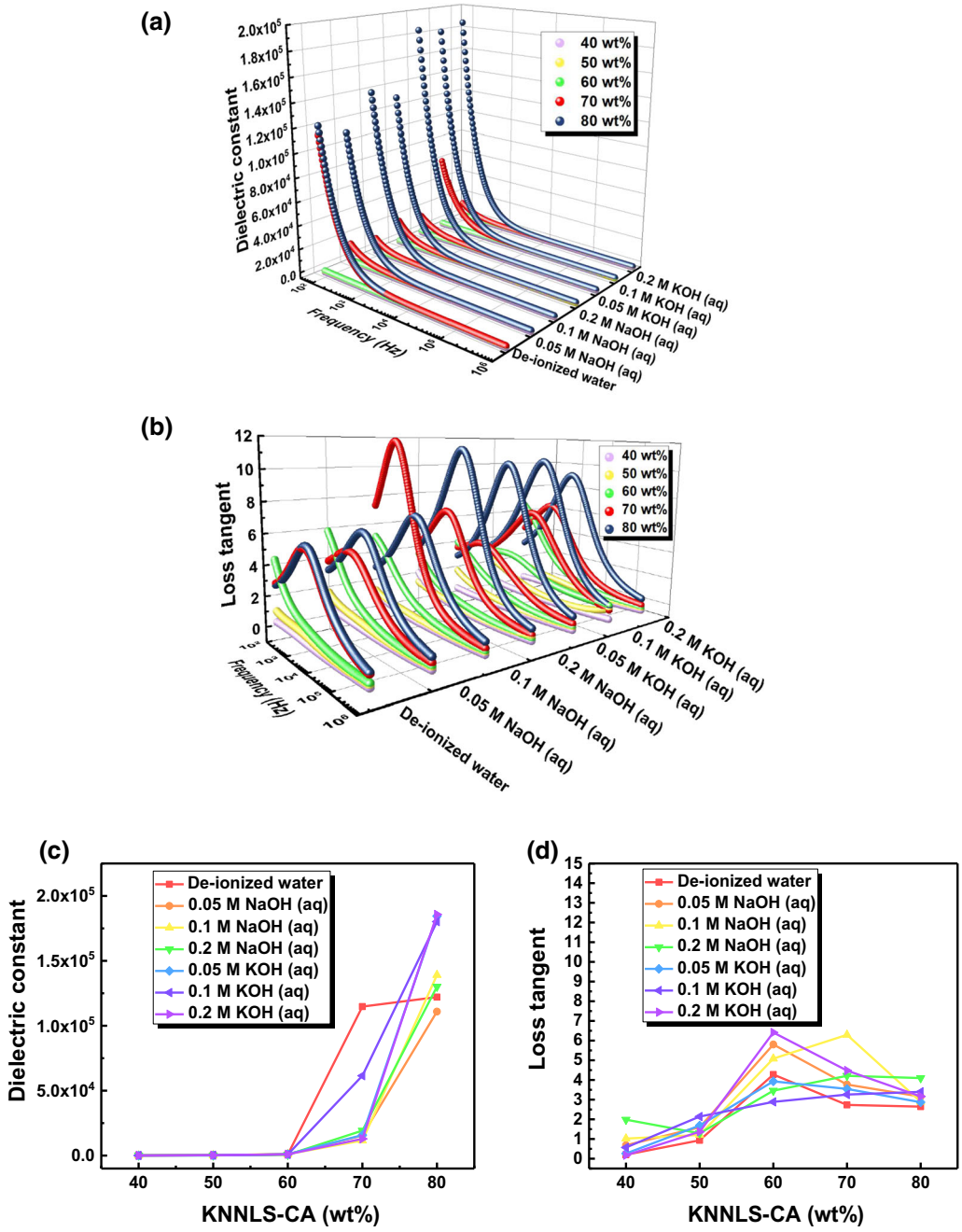

Fig. 6. Frequency dependence of (a) dielectric constant and (b) loss tangent of (KNNLS-CA)/PVDF composites with different weight fractions. (c) Dielectric constant and (d) loss tangent of (KNNLS-CA)/PVDF composites with different weight fractions at 100 Hz.

order to estimate the frequency stability, the following formula is used to calculate it.

$$S = \frac{\varepsilon_r(f = 100\,\text{Hz}) - \varepsilon_r(f = 1\,\text{MHz})}{\varepsilon_r(f = 100\,\text{Hz})} \times 100\%. \quad (7)$$

The result shows that when the ceramic content is 40%, 50%, 60%, 70% and 80%, the S is 20.8%, 25.2%, 32.0%, 42.2% and 62.3%, respectively. The phenomenon indicates that the frequency stability of the composite decreases with the increase of ceramic content.

Figure 5(b,d) show the dielectric constant and loss tangent increase with KNNLS-CA ceramic content in the composites at 100 Hz. When the ceramic content is 80%, the dielectric constant reaches a high value of 200, which is about 21 times higher than that of pure PVDF polymer, and the loss tangent reaches about 0.7. Generally speaking, when the ceramic content increases, because of the dielectric constant of ceramic is much higher than PVDF, it is understandable that the dielectric constant increases with the increase of

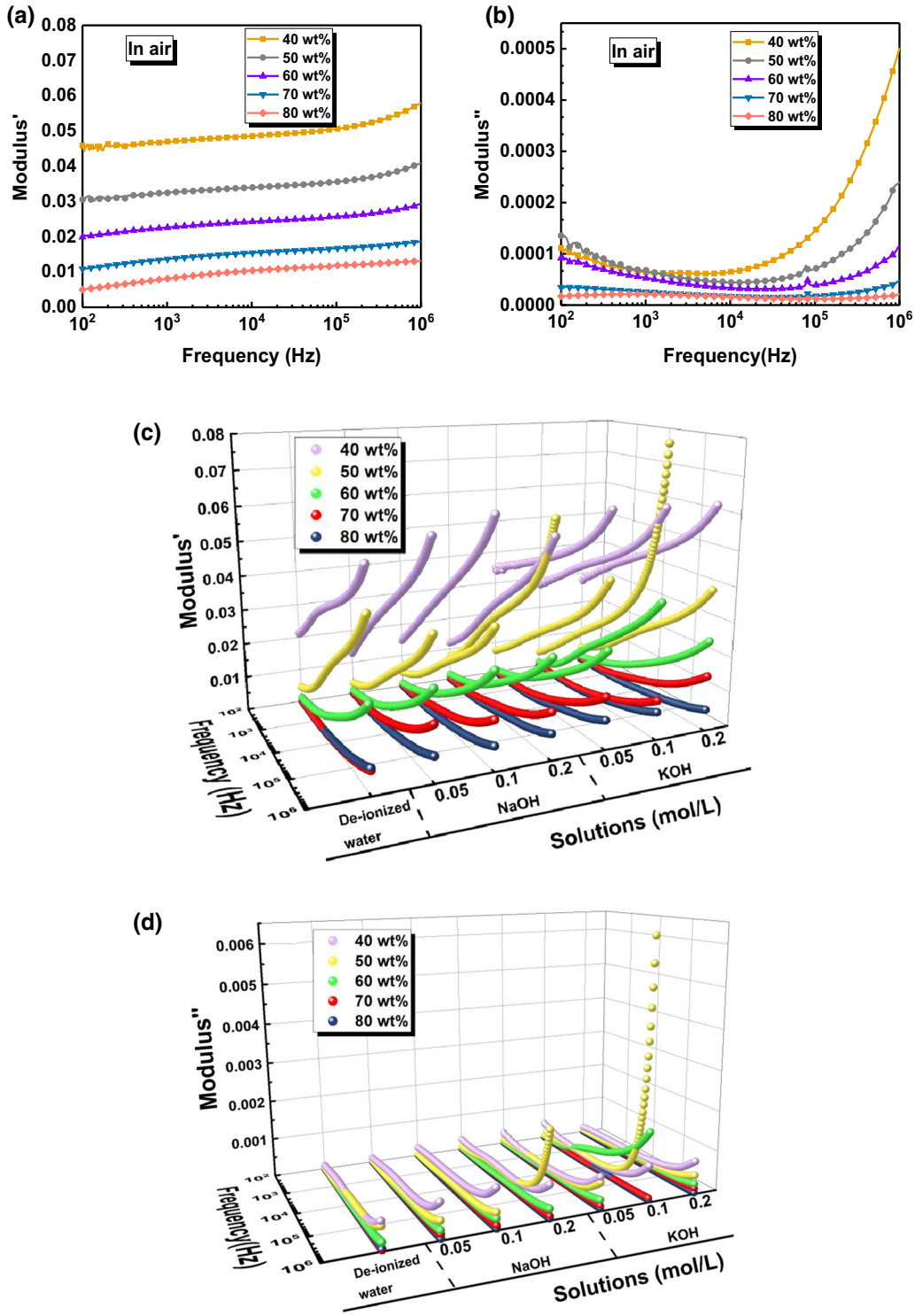

Fig. 7. In air (untreated): frequency dependence of the (a) real and the (b) imaginary components of the electric modulus of (KNNLS-CA)/PVDF composites with different weight fractions. In other immersing conditions: frequency dependence of the (c) real and the (d) imaginary components of the electric modulus of (KNNLS-CA)/PVDF composites with different weight fractions.

ceramic content. The loss tangent is mainly affected by two factors. First, it can be seen clearly that some micro pores on the surface of the composite with the increase of ceramic content from Fig. 3 SEM images, which lead to high loss tangent.[42] Second, the Maxwell–Wagner–Sillars (MWS) effect, when ceramic content increases, more conductive channels can be formed, high ceramic content can lead to the high loss tangent.[43,44]

Figure 6a displays the dielectric constants of the composites as a function of frequency which range from 10^2 Hz to 10^6 Hz after immersing 24 h in de-

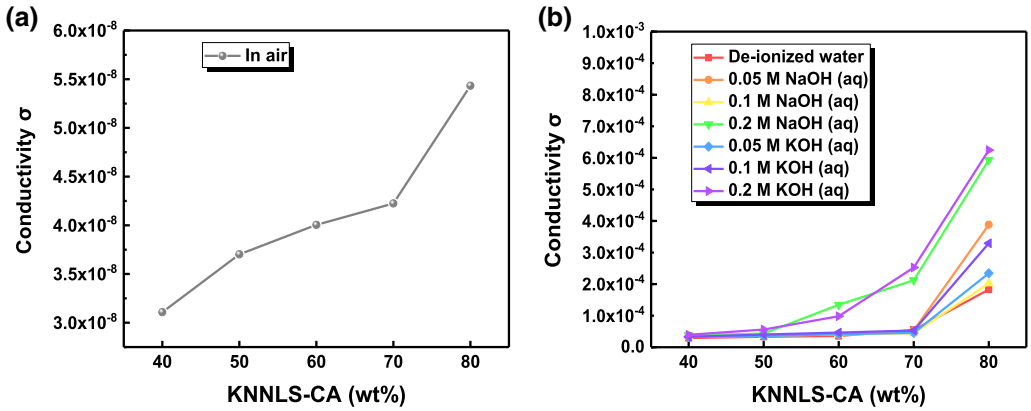

Fig. 8. Variations of the conductivity σ at 100 Hz with the weight of KNNLS-CA ceramic: (a) untreated samples and (b) samples were treated in different KOH/NaOH (aq) conditions.

ionized water and NaOH/KOH solutions of different concentrations. As expected, the dielectric constant decreases with increment of frequency, and increases with ceramic content in the composites. Surprisingly, a sharp increase of the dielectric constant is observed below 10^3 Hz when the ceramic weight fraction exceeded 60%. Figure 6c shows the dielectric constant increases with ceramic content in the composites at 100 Hz. When the ceramic content reaches 60%, the ε_r increases sharply. In particular, the dielectric constant (De-ionized water) reaches an ultrahigh value of 122,040 when the ceramic content is 80%, which is about 610 times higher than that of the composites without dipped in de-ionized water (Fig. 5b). Even at 1 kHz, the dielectric constant also can reach 9336. On the other hand, the dielectric constant of the sample treated with 0.2 M KOH (aq) can reach an ultrahigh value of 185,723, even at 1 kHz, the dielectric constant also can reach 11,266.

Figure 6b displays the loss tangents of the composites as a function of frequency which range from 10^2 Hz to 10^6 Hz after immersing 24 h in de-ionized water and NaOH/KOH solutions of different concentrations. It is interesting to note that when the ceramic content is above 60%, the loss tangent increases with increment of frequency, and reaches a maximum value at around 10^4 Hz. This phenomenon can be ascribed to the glass transition relaxation of the PVDF polymer matrix or denoted as α relaxation process.[5,45,46] Molecular friction caused by relaxation polarization of dipoles would give rise to increased loss tangent.[47] Further, in order to investigate the α relaxation process, the following frequency dependent electrical modulus formalism are used:[48]

$$M' = \frac{\varepsilon'}{\varepsilon'^2 + \varepsilon''^2}, \tag{8}$$

$$M'' = \frac{\varepsilon''}{\varepsilon'^2 + \varepsilon''^2}, \tag{9}$$

$$M^* = M' + iM'' = \frac{1}{\varepsilon^*}, \tag{10}$$

where M' is the real component of the electric modulus, M'' is the imaginary component of the electric modulus, ε' and ε'' are the real and imaginary components of the dielectric constant. In Fig. 7(a and c), it is shown that the real component of electric modulus M' decreases with the addition of the ceramic in the composite because of the enhanced dielectric constant.[48,49] On the other hand, the α relaxation process is also observed in Fig. 7(b and d) and the imaginary part of electric modulus M'' increases with increment of frequency. This phenomenon may influence a polarization effect (this causes electric charge accumulation around the ceramic associated with PVDF).[50] However, there are some controversy about the origin of α relaxation process. Some researchers attribute this process to the micro-Brownian motions of the main chain backbone or the amorphous phase chain segments (in other words, above the glass transition temperature, T_g, the molecules of this phase have sufficient mobility to orient the dipoles under the action of an electric field),[51,52] and others to the movement of crystalline amorphous interphase chain segments.[53,54]

The loss tangent changes with ceramic content in the composites at 100 Hz are shown in Fig. 6d. When the ceramic content is 60%, the loss tangent of the samples immersed in de-ionized water, 0.05 M NaOH (aq), 0.05 M KOH (aq) and 0.2 M KOH (aq) reaches a maximum value (4.28, 5.80, 3.93 and 6.41). When the ceramic content is 70%, the loss tangent of the samples soaked by 0.1 M NaOH (aq) and 0.2 M NaOH (aq) reaches the maximum value (6.29 and 4.21). However, the loss tangent of the samples soaked by 0.1 M KOH (aq) increases with the ceramic content all the time.

The conductivity σ (at 100 Hz) of samples are shown in Fig. 8, the conductivity σ increases with ceramic content in the composites. However,

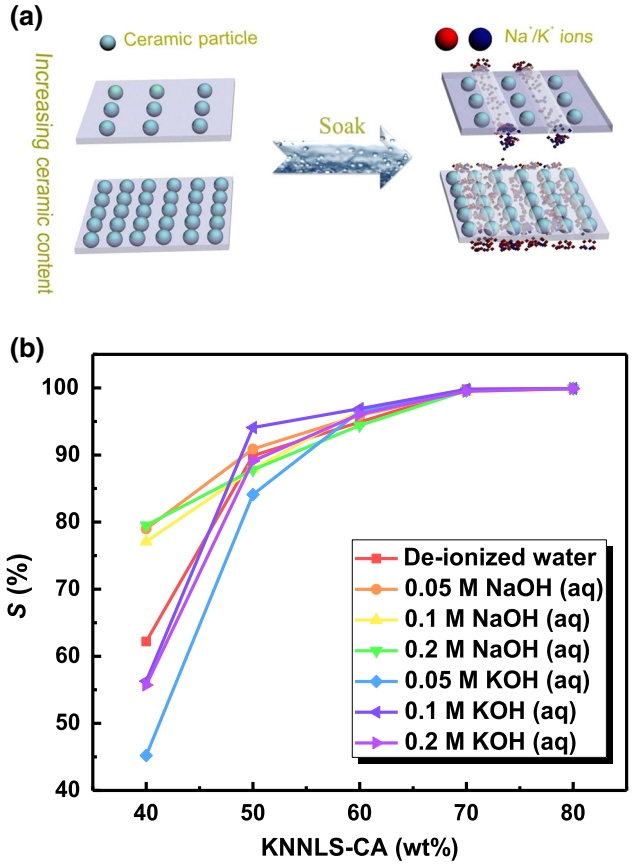

Fig. 9. (a) The formation of conductive channel. (b) The *S* of samples were soaked with de-ionized water and NaOH/KOH (aq) at various concentrations.

comparing with the conductivity σ of untreated samples, when the samples were treated in de-ionized water or other solutions, it increased by several orders of magnitude. It also can be seen clearly that when the weight fraction of ceramic increased from 70% to 80% (the corresponding volume fractions were given above), the dielectric constant of the untreated (Fig. 5b) and treated (Fig. 6c) samples increases dramatically. This phenomenon can be explained by the percolation theory. When the samples become percolative capacitors, their dielectric constant follows the Eq. 11:

$$\varepsilon_r = \varepsilon_m \left| \frac{f_c - f_{\mathrm{KNNLS-CA}}}{f_c} \right|^{-q}, \qquad (11)$$

where ε_m is the dielectric constant of the matrix, $f_{\mathrm{KNNLS-CA}}$ is the volume fraction of the KNNLS-CA ceramic, f_c is the percolation threshold which is of guiding significance for the preparation and use of electronic devices, and q is the dielectric critical exponent of about 1. When f approaches f_c, the dielectric constant can increase exponentially. When the interface percolation has formed (near the percolation threshold), the conductivity σ of

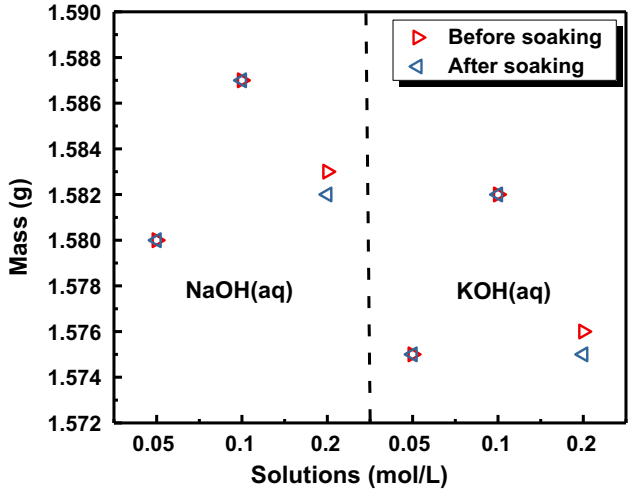

Fig. 10. The average mass of the samples before and after soaking at different environments.

samples in increases with volume fraction of ceramic in the composites.

Moreover, after soaking 24 h in de-ionized water and NaOH/KOH solutions, the dielectric constant and loss tangent are much higher than those of untreated samples. There are two main reasons for this phenomenon. First, as is known to all, internal stresses can be formed of micro cracks due to cooling after hot-pressing, and may be continue to form after poling. The water and aqueous solution can promote crack growth and isolate the grains, therefore, the dielectric constant and loss tangent are greatly increased after treatment.[55] On the other hand, ceramic particles consist of many grains with insulating potential barriers of each grain boundary. When water enters the composite, the ions (like K^+ and Na^+ ions from ceramic or solution) can form a conductive channel (as shown in Fig. 9a) at the grain boundary (the MWS effect as mentioned above), which leads to the insulating potential barriers in the grain boundaries are weakened, and eventually the dielectric constant and loss tangent increase sharply.[56,57] It is important to note that the dielectric constant and loss tangent (NaOH/KOH solutions) are significantly higher than those of samples that were treated with de-ionized water. This may be because of K^+ and Na^+ ions can promote the formation of conductive channels, and there are many free ions in the solution which lead to high conductivity. Interestingly, the dielectric constant of samples that were treated with KOH (aq) is higher than that of samples treated with NaOH (aq), which may be correlated with K^+ ions are easier to form electrolytes and become a conductive phase. According to the Eq. 7, the *S* of samples soaked with de-ionized water and NaOH/KOH (aq) at various concentrations is shown in Fig. 9b. As expected, the frequency stability decreases as the ceramic content increases. When the ceramic content exceeds 60 wt.%, the *S* value

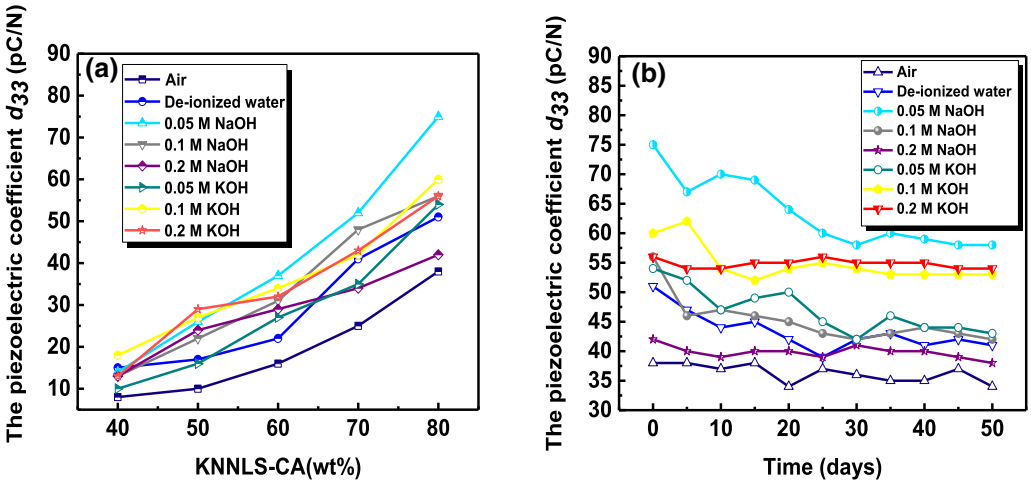

Fig. 11. (a) The piezoelectric coefficients d_{33} of samples treated different conditions. (b) Dependence of the piezoelectric coefficients d_{33} of the all 80/20 samples on time.

tends to be consistent. Similar to air, de-ionized water and NaOH/KOH (aq) can seriously interfere with the frequency stability.

Piezoelectric Properties

The samples were soaked in these strong base solutions and removed, there is no visible corrosion. Figure 10 shows the average mass of the samples before and after soaking at different environments. We can see obviously that the samples appear in mass change only at relatively high concentrations (0.2 M). It may due to 0.2 M solutions caused the destruction on PVDF and the organic components of the silver paste. Alkali solutions can affect the mechanical properties of PVDF, such as Young's modulus and elongation at break, and cause dehydrofluorination.[58] However, the dehydrofluorination process normally occur at the peaks at a range of 1590–1650 (carbon–carbon double bond), 1700–1800 (carbonyl bond) and 2100 cm^{-1} (carbon–carbon triple bond).[59,60] This does not affect the ratio of the β-phase (840, 871, 1070, 1276 and 1401 cm^{-1}) and the piezoelectric properties of PVDF.

Figure 11a shows the piezoelectric coefficients d_{33} of the samples soaked under different conditions. It is obvious that the d_{33} of the samples immersed in de-ionized water and NaOH/KOH solutions is much higher than that of the samples normally placed in the air. It is surprising that when the ceramic content is 80%, the d_{33} of the sample immersed in 0.05 M NaOH (aq) can reach the high value of 75 pC/N. The results indicate that the de-ionized water and NaOH/KOH solutions can greatly improve the piezoelectric property. This may be because the solution dissolves the free alkali metal ions, such as K^+ and Na^+ ions, produced by the deliquescen ce of KNNLS-CA ceramic, or these ions are ingenerate in the solution. Generally speaking, in air, the alkali metal ions from deliquescence of ceramic particles neutralize the space charges andcan lead to weaken the piezoelectric property of the samples.[10] Hence, untreated samples usually have lower d_{33} values, but, however, the ions can dissolved in the trace solution inside a sample, resulting in that these ions cannot neutralize space charges. Therefore, the piezoelectric coefficient of the immersed sample is higher than that of untreated sample. In order to investigate stability of the piezoelectric property of the samples which contain 80% ceramic components, the piezoelectric coefficient d_{33} of the samples was measured at 22–27°C at multiple time points. Figure 11b shows the dependence of the piezoelectric coefficients d_{33} of the all 80/20 samples on time. It can be observed that, in 50 days, the piezoelectric coefficient of all samples decreased slightly over time. As for this phenomenon, this is because the water gradually volatilized after exposure to the air for a period of time, and the alkali metal ions attach to the sample and neutralize the space charges. This is why the piezoelectric coefficient of those samples decreases respectively to a nearly stable value with time when they are exposed in air.

CONCLUSIONS

The $0.970(0.95(K_{0.485}Na_{0.515})\ NbO_3\text{-}0.05LiSbO_3)\text{-}0.015CuO\text{-}0.015Al_2O_3$ ceramic was prepared by the conventional solid state reaction, then (KNNLS-CA)/PVDF composites were fabricated by the hot-pressing process. The XRD pattern of composites mainly shows the peaks of KNNLS-CA ceramic, and the phase structure is perovskite with orthorhombic symmetry. KNNLS-CA ceramic particles can influence crystallite size and lattice strain of composites. FTIR study carried out on the composite confirmed the ceramic particles can increase the ratio of the β-phase in composites. The ceramic particles and most elements are well dispersed in polymer matrix by SEM–EDS. Comparing with the dielectric constant, loss tangent and piezoelectric coefficient of the samples which were placed in air, the above

properties of the samples which were soaked by deionized water and NaOH/KOH (aq) are improved significantly. Among all samples, the dielectric constant of the samples (80 wt.%) which were immersed in 0.2 M KOH (aq) can reach 185,723 at 100 Hz. The dielectric properties are well explained in terms of an interfacial percolation model. The piezoelectric coefficient of the samples (80 wt.%) which were immersed in 0.05 M NaOH (aq) can reach 75 pC/N, and the aging experiment shows that the composites have a good stability in piezoelectric properties.

ACKNOWLEDGMENTS

This work was supported by Science and Technology development Fund of China University of Geosciences (Grant No. 110-KH14J130).

CONFLICT OF INTEREST

The authors declare that there is no conflict of interests regarding the publication of this article.

REFERENCES

1. L. Wu, J.L. Zhang, C.L. Wang, and J.C. Li, *J. Appl. Phys.* 103, 45 (2008).
2. Z. Tan, J. Xing, J. Wu, Q. Chen, W. Zhang, J. Zhu, and D. Xiao, *J. Mater. Sci. Mater. Electron.* 29, 5337 (2018).
3. P. Li, X.Q. Chen, F.F. Wang, B. Shen, J.W. Zhai, S.J. Zhang, and Z.Y. Zhou, *ACS Appl. Mater. Interfaces* 10, 28772 (2018).
4. J. Ma, B. Wu, W.J. Wu, and M. Chen, *J. Mater. Sci. Mater. Electron.* 29, 12323 (2018).
5. J.Q. Lin, G.R. Chen, W.L. Yang, H. Li, and Q.Q. Lei, *J. Polym. Res.* 23, 143 (2016).
6. M. Olszowy, E. Nogas-Cwikiel, and K. Cwikiel, *J. Phys: Conf. Ser.* 289, 12017 (2011).
7. S.K. Pradhan, A. Kumar, A.N. Sinha, P. Kour, R. Pandey, P. Kumar, and M. Kar, *Ferroelectrics* 516, 18 (2017).
8. D.Q. Zhang, D.W. Wang, J. Yuan, Q.L. Zhao, Z.Y. Wang, and M.S. Cao, *Chin. Phys. Lett.* 25, 4410 (2008).
9. M. Kato and K.I. Kakimoto, *Mater. Lett.* 156, 183 (2015).
10. P.Y. Zhang, M.S. Wang, J.L. Zhu, and X.J. Zhu, *J. Mater. Sci. Mater. Electron.* 25, 4225 (2014).
11. W.S. Rosa, M. Venet, J.C. M'Peko, H. Amorin, and M. Alguero, *J. Alloys Compd.* 744, 691 (2018).
12. W.Y. Li, Z.Q. Song, J. Qian, H.Y. Chu, X.Y. Wu, Z.Y. Tan, and W. Nie, *Ceram. Int.* 44, 4835 (2018).
13. L. Wang, F. Gao, J. Xu, K.N. Zhang, J. Kong, M. Reece, and H.X. Yan, *Compos. Sci. Technol.* 158, 112 (2018).
14. J. Tolvanen, J. Hannu, M. Nelo, J. Juuti, and H. Jantunen, *Smart Mater. Struct.* 25, 9 (2016).
15. R.K. Goyal and A.B. Kulkarni, *J. Phys. D Appl. Phys.* 45, 46 (2012).
16. K. Yu, H. Wang, Y.C. Zhou, Y.Y. Bai, and Y.J. Niu, *J. Appl. Phys.* 113, 321 (2013).
17. A.K. Zak, W.C. Gan, W.H. Abd Majid, M. Darroudi, and T.S. Velayutham, *Ceram. Int.* 37, 1653 (2011).
18. B. Ponraj, R. Bhimireddi, and K.B.R. Varma, *J. Adv. Ceram.* 5, 308 (2016).
19. T. Lusiola, A. Hussain, M.H. Kim, T. Graule, and F. Clemens, *Actuators* 45, 2344 (2015).
20. Y.Q. Huang, H.W. Du, W. Feng, H.N. Qin, and Q.B. Hu, *J. Alloys Compd.* 590, 435 (2014).
21. C. Chen, Y. Huang, Y. Tan, and Y. Sheng, *J. Alloys Compd.* 663, 46 (2016).
22. Y. Guo, K.-I. Kakimoto, and H. Ohsato, *Appl. Phys. Lett.* 85, 4121 (2004).
23. H. Abdoli, E. Salahi, H. Farnoush, and K. Pourazrang, *J. Alloys Compd.* 461, 166 (2008).
24. S. Ayed, R. Ben Belgacem, J.O. Zayani, and A. Matoussi, *Superlattices Microstruct.* 91, 118 (2016).
25. M. Razavi, M.R. Rahimipour, T. Ebadzadeh, S.S.R. Tousi, and B. Mater, *Science* 32, 155 (2009).
26. B. Nasiri-Tabrizi and A. Fahami, *Ceram. Int.* 39, 4329 (2013).
27. S. Garehbaghi and A. Kianvash, *Results Phys.* 12, 1559 (2019).
28. P. Kour and S.K. Sinha, *Cerâmica* 59, 34 (2013).
29. G.K. Williamson and W.H. Hall, *Acta Metall. Mater.* 1, 23 (1953).
30. L. Yu and P. Cebe, *Abstr. Pap. Am. Chem Soc.* 238, 34 (2009).
31. V. Tiwari and G. Srivastava, *Ceram. Int.* 41, 8008 (2015).
32. J.S. Andrew and D.R. Clarke, *Langmuir* 24, 670 (2008).
33. M.P. Silva, C.M. Costa, V. Sencadas, A.J. Paleo, and S. Lanceros-Mendez, *J. Polym. Res.* 18, 1451 (2011).
34. S.H. Cho and Y.J. Yoon, *J. Korean Phys. Soc.* 68, 340 (2016).
35. S.T. Wang, J. Sun, L. Tong, Y.M. Guo, H. Wang, and C.C. Wang, *Mater. Lett.* 211, 114 (2018).
36. J.H. Seol, J.S. Lee, H.N. Ji, Y.P. Ok, G.P. Kong, K.S. Kim, C.Y. Kim, and W.P. Tai, *Ceram. Int.* 38, 263 (2012).
37. Z.M. He, J. Ma, R.F. Zhang, and T. Li, *J. Eur. Ceram. Soc.* 23, 1943 (2003).
38. T. Kar, J. Mal, and R.N.P. Choudhary, *J. Mater. Sci. Lett.* 16, 328 (1997).
39. Y. Chen, S.X. Xie, H.M. Wang, Q. Chen, Q.Y. Wang, J.G. Zhu, and Z.W. Guan, *J. Alloys Compd.* 696, 746 (2017).
40. N. Marimuthu, R. Parasuraman, M. Rathnakumari, P. Kumar, and R. Upadhyay, *J. Mater. Sci. Mater. Electron.* 29, 1280 (2018).
41. K.T. Selvi, K. Alamelumangai, M. Priya, M. Rathnakumari, P.S. Kumar, and S. Sagadevan, *J. Mater. Sci. Mater. Electron.* 27, 6457 (2016).
42. E. Roncari, C. Galassi, F. Craciun, C. Capiani, and A. Piancastelli, *J. Eur. Ceram. Soc.* 21, 409 (2001).
43. Z.M. Dang, T. Zhou, S.H. Yao, J.K. Yuan, J.W. Zha, H.T. Song, J.Y. Li, Q. Chen, W.T. Yang, and J. Bai, *Adv. Mater.* 21, 2077 (2009).
44. Y. Yang, B.P. Zhu, Z.H. Lu, Z.Y. Wang, C.L. Fei, D. Yin, R. Xiong, J. Shi, Q.-G. Chi, and Q.Q. Lei, *Appl. Phys. Lett.* 102, 42904 (2013).
45. C.V. Chanmal and J.P. Jog, *Express Polym. Lett.* 2, 294 (2008).
46. R. Gregorio and E.M. Ueno, *J. Mater. Sci.* 34, 4489 (1999).
47. Y.H. Li, J.J. Yuan, J. Xue, F.Y. Cai, F. Chen, and Q. Fu, *Compos. Sci. Technol.* 118, 198 (2015).
48. P. Thomas, S. Satapathy, K. Dwarakanath, and K.B.R. Varma, *Express Polym. Lett.* 4, 632 (2010).
49. P.I. Devi and K. Ramachandran, *J. Exp. Nanosci.* 6, 281 (2011).
50. R. Aepuru and H.S. Panda, *J. Phys. Chem. C* 118, 18868 (2014).
51. A. Bello, E. Laredo, and M. Grimau, *Phys. Rev. B* 60, 12764 (1999).
52. K. Nakagawa and Y. Ishida, *J. Polym. Sci.* 11, 1503 (1973).
53. B. Hahn, J. Wendorff, and D.Y. Yoon, *Macromolecules* 18, 718 (1985).
54. T. Ando, T. Hanada, and K. Saitoh, *J. Polym. Sci. Pol. Phys.* 32, 179 (1994).
55. M. Kosec, B. Malic, W.W. Wolny, A.S. James, C. Alemany, and L. Pardo, *J. Korean. Phys. Soc.* 32, 1163 (1998).
56. W.P. Chen and H.L.W. Chan, *Jpn. J. Appl. Phys.* 43, 701 (2004).

57. S. Riaz, Sajid-Ur-Rehman, M. Abutalib, and S. Naseem, *J. Electron. Mater.* 45, 5185 (2016).
58. M.F. Rabuni, N.M.N. Sulaiman, M.K. Aroua, and N.A. Hashim, *Ind. Eng. Chem. Res.* 52, 15874 (2013).
59. N.A. Hashim, Y.T. Liu, and K. Li, *Chem. Eng. Sci.* 66, 1565 (2011).
60. S.C. Zhang, J. Shen, X.P. Qiu, D.S. Weng, and W.T. Zhu, *J. Power Sources* 153, 234 (2006).